Acta Geotechnica (2022) 17:2347–2363
https://doi.org/10.1007/s11440-021-01398-0

RESEARCH PAPER

Extended model of shear modulus reduction for cohesive soils

John Kok Hee Wong[1] · Soon Yee Wong[1] · Kim Yuen Wong[2]

Received: 20 January 2021 / Accepted: 10 October 2021 / Published online: 30 November 2021

Abstract

The shear modulus of a soil, G, shows a hyperbolic degradation curve relationship with increasing shear strain, γ. G is usually normalized against the small-strain modulus (G_{max}) as G/G_{max} vs γ (log). Factors that significantly influence G are shear strain amplitude, γ, soil plasticity index (PI) and effective pressure, σ'. Design curve charts of G/G_{max} vs γ have been produced for seismic engineering purposes. Mathematical models have also been developed, using statistically analysed parameters to reflect the influence of γ, PI and σ'. Soil overconsolidation ratio (OCR) has a significantly lesser impact than the three mentioned factors. In this paper, mathematical fitting and shaping functions for PI and σ' are developed to extend the shear modulus reduction model further. The requirement to calculate reference strain, $\gamma_{ref,}$ is removed, and only soil PI and σ' are required. Cyclic triaxial experiments are conducted with reconstituted kaolin and bentonite in different mix proportions (to achieve varying PI) and at different effective stresses. The model equation matches well against both the established curves and experimental results and can facilitate preliminary prediction of shear stress–strain behaviour and G_{max} with different cohesive soil types and at different depths below ground.

Keywords Bentonite · Cohesive soils · Effective pressure · Kaolin · Modulus degradation curve · Plasticity index · Shear modulus

List of symbols

B	Bentonite
D	Damping ratio, soil
E	Elastic modulus, soil
e	Void ratio, soil
G_{max}	Very small-strain shear modulus, soil
G	Shear modulus, soil
G/G_{max}	Normalized shear modulus vs shear strain curve
K	Kaolin
OCR	Overconsolidation ratio, soil
PI	Plasticity index, soil
UCS	Unconfined compressive strength (q_{uc})
σ'	Effective stress, soil
σ_D	Deviatoric stress, soil
α	Power factor curvature parameter
ε	Axial strain
γ	Shear strain
$\gamma_{0.7}$	Shear strain at $G/G_{max} = 0.7$
ν	Poisson ratio
$f(\sigma')$	Fitting function (effective pressure)
f(PI)	Fitting function (plasticity index)
Z	Curvature function (effective pressure)
atm	Atmospheric pressure

1 Introduction

While the soil elastic modulus (E) defines elastic behaviour due to axial loading, the shear modulus identifies a soil's deformation due to shear loading. The shear modulus (G) and damping ratio (D) are the two primary soil properties utilized in seismic analysis to predict response to dynamic loading. It is also known that cyclic secant shear modulus G degrades nonlinearly with increasing shear strain (γ), hence the importance of the shear modulus or stiffness vs shear strain relationship. The shear stiffness is often normalized to the very small-strain modulus, G_{max}, as a ratio of G/G_{max} to provide a dimensionless predictive

✉ John Kok Hee Wong
evxjw1@nottingham.edu.my

[1] Department of Civil Engineering, University of Nottingham Malaysia, Jalan Broga, 43500 Semenyih, Selangor, Malaysia

[2] Soilpro Technical Services Sdn Bhd, 16, Jalan TIB-1/17, Taman Industri Bolton, 68100 Batu Caves, Selangor, Malaysia

value of the shear stiffness with increasing shear strain values, irrespective of the G_{max} values measured.

As shown in Fig. 1, the normalized shear modulus curve can be organized into three main sections, which are separated by threshold shear strain points:

- Very small strains ($\gamma < 0.001\%$), where the shear modulus is generally constant and maximum.
- Small to medium strains ($0.001 < \gamma < 0.1\%$) where shear modulus begins to degrade in nonlinear fashion.
- Large strains ($\gamma > 0.1\%$), where strength degradation is non-recoverable, and the soil eventually reaches failure.

To derive the normalized curve, it is usually necessary to obtain the very small-strain shear modulus (G_{max}), which requires either bender element or resonant column tests in the laboratory or from field measurements of shear wave velocity (i.e. $G_{max} = \rho V_s^2$). Correlation studies by Karray and Hussein [7] between normalized tip resistance and shear wave velocity may also lead to the development of Gmax from CPT results. However, bender element tests measure shear strains up to 0.001% and resonant column tests, up to 0.1%. The larger strain measurements require cyclic triaxial tests.

Many empirical equations soils have been developed and compiled to estimate G_{max} for cohesive based on void ratio (e), effective stress (σ'), overconsolidation ratio (OCR) and plasticity index (PI) [6].

Previous researchers have developed regression models from experimental results to aid in design. Hardin and Drnevich [3] developed the basic hyperbolic model upon which many subsequent models are based. Vucetic and Dobry [21] created design charts showing the effect of PI on modulus reduction curve (G/G_{max}) vs shear strain (γ). Ishibashi and Zhang [4] proposed a unified formula for shear modulus from the analysis of experimental research data of various soils, from non-plastic sands to highly plastic clay. Subsequently, Darendeli [1] and Zhang et al. [23] both introduced a shaping power parameter (α) to the normalized shear strain (γ/γ_{ref}) in Hardin and Drnevich's model to better fit the normalized curve for small strains. Vardanega and Bolton [20] proposed an alternative way to estimate Darendeli's power parameter (α) by transforming the hyperbolic equation to a linear form for ease of regression analysis. Finally, Kishida et al. [10] developed a shear modulus regression model for highly organic soils and subsequently proposed an adaptation for cohesive soils [8, 9].

This article proposes further development of the normalized shear modulus regression model to a form that requires only the following primary influence factors to be input—cyclic shear strain (γ_c), plasticity index (PI) and effective stress (σ'). A series of strain-controlled cyclic

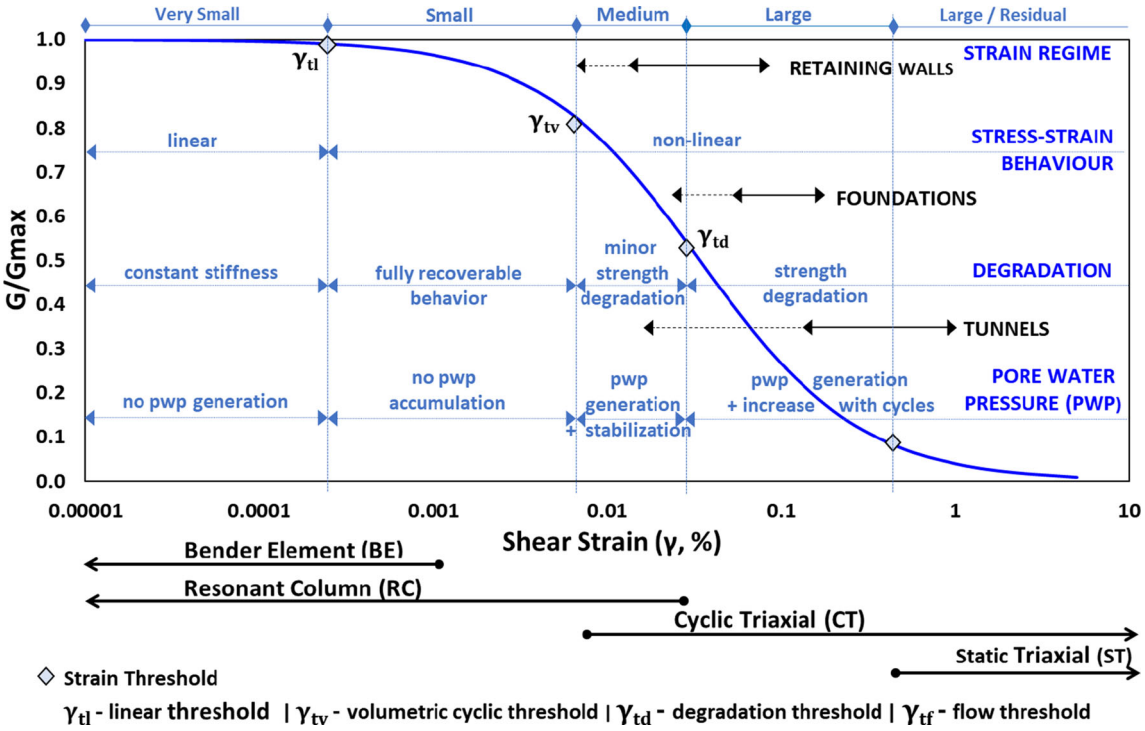

Fig. 1 Normalized shear modulus (G/G_{max}) vs shear strain showing strain range classification, stress–strain behaviour, type of degradation and pore pressure state. Also shown are the typical strain ranges related to different soil behaviour and laboratory equipment measurement ranges. Adapted from [2, 16]

triaxial experiments of reconstituted soils of varying PI and at different σ' are conducted to validate the model.

2 Discussion of models for normalized shear modulus vs shear strain

This section summarizes how different regression models address the key influence variables of shear strain (γ), plasticity index (PI) and effective stress (σ').

2.1 Hardin and Drnevich [3]

Hardin and Drnevich [3] defined the normalized shear modulus model as a hyperbolic relationship.

$$\frac{G}{G_{max}} = \frac{1}{\left(1 + \frac{\gamma}{\gamma_{ref}}\right)} \tag{1}$$

whereby γ_{ref} is taken as shear strain at $G/G_{max} = 0.5$.

The above model is a symmetrical sigmoidal function. The reference strain determines the location of the midway point of the curve. However, the primary influence factors of PI, σ', are not directly considered in the model.

2.2 Vucetic and Dobry [21]

Subsequently, Vucetic and Dobry [21] studied the correlation between G/G_{max} and PI. They used cohesive soils of various PI from a database of 16 studies to develop the ready-to-use design curves for cohesive soils of various PI. The constructed trend lines of six PIs to different strains and G/G_{max} values are generated for each PI. No significant influence was detected in the G/G_{max} values for a wide range of OCR from 1 to 15. However, the effect of effective stress was not considered in the design curves [4]. Furthermore, findings are represented graphically without the benefit of an equation as shown in Fig. 2. Hence, interpolation between the six defined curves and extrapolation to obtain values beyond the 1% strain is required.

2.3 Ishibashi and Zhang [4]

Ishibashi and Zhang [4] had proposed a simple unified formula that included non-plastic granular soils and highly plastic cohesive soils. Thus, their G/G_{max} is expressed in terms of (1) shear strain, (2) mean effective pressure and (3) soil plasticity index.

$$\frac{G}{G_{max}} = K\left(\gamma, I_p\right)\sigma_{m0}^{'\overset{\vee}{m}\left(\gamma, I_p\right)} \tag{2}$$

where,

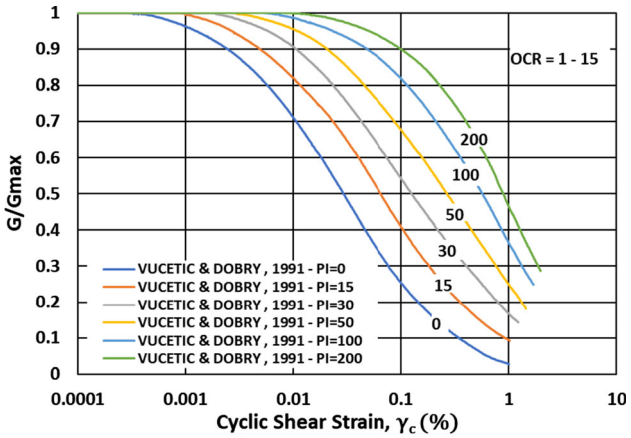

Fig. 2 Normalized shear modulus (G/G_{max}) vs shear strain for soils with different PI. Adapted from Vucetic and Dobry (1991) Fig. 6a [21]

$$\begin{aligned}
I_p &= \text{Plasticity index } (PI) \text{ expressed numerically}\\
K_o &= \text{coefficient of earth pressure at rest, which can}\\
&\quad \text{be considered as} \frac{1-v}{v} \text{and } v = \text{Poisson ratio}\\
\sigma_{v0}^{'} &= \text{effective vertical stress}\\
K\left(\gamma, I_p\right) &= 0.5\left[1 + \tanh\left\{ln\left(\frac{0.000102 + n\left(I_p\right)}{\gamma}\right)^{0.492}\right\}\right]\\
n\left(I_p\right) &= 0 \quad \text{for} \quad I_p = 0\\
&= 3.37 \cdot 10^{-6} I_p^{1.404} \quad \text{for} \quad 0 < I_p \le 15\\
&= 7.0 \cdot 10^{-7} I_p^{1.976} \quad \text{for} \quad 15 < I_p \le 70\\
&= 2.7 \cdot 10^{-5} I_p^{1.115} \quad \text{for} \quad I_p > 70\\
\overset{\vee}{m}\left(\gamma, I_p\right) &= 0.272\left[1 - \tanh\left\{ln\left(\frac{0.000556}{\gamma}\right)^{0.4}\right\}\right] e^{-0.0145 I_p^{1.3}}\\
\sigma_{m0}^{'} &= \text{mean in situ effective stress}\\
&= \left(\frac{1 + 2K_o}{3}\right)\sigma_{v0}^{'}
\end{aligned} \tag{3}$$

The formula was developed from a general equation for sandy soils adapted from research by Hardin and Drnevich [3], Iwasaki et al. [5], Tatsuoka et al. [18] and Kokusho [11] from the form $G = K(\gamma)\bar{\sigma}_{m0}^{\overset{\vee}{m}(\gamma)}$. The equation is then adapted to include plasticity index effects.

2.4 Darendeli [1]

From a database of 110 resonant column and torsional shear tests from twenty different sites in four separate geographic locations, Darendeli's [1] PhD research utilizes Hardin and Drnevich's hyperbolae function. The soil samples' PI ranges from non-cohesive, i.e. 0 to 132%. In

addition, a curvature coefficient power factor (α) is inserted into the normalized shear strain equation to fit the soil results better.

$$\frac{G}{G_{max}} = \frac{1}{1 + \left(\frac{\gamma}{\gamma_r}\right)^{\alpha}} \tag{4}$$

where,

$$\gamma_r = \left(\varnothing 1 + \varnothing 2 \cdot \mathrm{PI} \cdot \mathrm{OCR}^{\varnothing 3}\right) \cdot \sigma_o^{'\varnothing 4}$$
$$\alpha = \varnothing 5$$

The following parameters, Ø1 to Ø5 for the regression model, are obtained using the first-order, second-moment Bayesian method.

$$\varnothing 1 = 0.0352;\ \varnothing 2 = 0.0010;\ \varnothing 3 = 0.3246$$
$$\varnothing 4 = 0.3483;\ \varnothing 5 = 0.919$$

2.5 Zhang et al. [23]

Zhang et al. [23] developed equations for estimating the curvature parameter power factor (α), and for reference strain (γ_r) of Quaternary, Tertiary and older, and residual/saprolite soils from statistical analysis of resonant column and torsional shear test results of 122 specimens from South Carolina, North Carolina and Alabama, USA. Influence factors considered in Zhang et al.'s equations are shear strain, mean effective confining stress and plasticity index. The modified hyperbolic model by Darendeli is still adopted as the modelling function, and the derived values α and γ_r that best fit Eq. (4) to the compiled test data are determined by multiple regression.

$$\begin{aligned}
\alpha &= 0.0021PI + 0.834 \quad \text{(Quaternary soil)} \\
&\qquad r^2 = 0.505 \\
&= 0.0009PI + 1.026 \quad \text{(Tertiary soil)} \\
&\qquad r^2 = 0.015 \\
&= 0.0043PI + 0.794 \quad \text{(Residual/Saprolite soil)} \\
&\qquad r^2 = 0.053
\end{aligned}$$

$$\mathrm{PI} = \text{Plasticity index (PI) numerically, } e.g.\ 0.4$$

$$\gamma_r = \gamma_{r1}\left(\sigma_m^{'}/P_a\right)^k$$

$$\gamma_r = \text{shear strain at } G/G_{max} = 0.5.$$

(5)

where,

γ_{r1} = reference strain at mean effective confining stress of 100 kPa

$$\begin{aligned}
&= 0.0011PI + 0.0749 \text{(Quaternary soil)} \quad r^2 = 0.508 \\
&= 0.0004PI + 0.0311 \text{(Tertiary soil)} \quad r^2 = 0.143 \\
&= 0.0009PI + 0.0385 \text{(Residual/Saprolite soil)} \\
&\quad r^2 = 0.107
\end{aligned}$$

P_a = reference stress of 100 kPa

k = stress correction exponent

$$\begin{aligned}
&= 0.316e^{-0.0142PI} \text{(Quaternary soil)} \quad r^2 = 0.323 \\
&= 0.316e^{-0.0110PI} \text{(Tertiary soil)} \quad r^2 = 0.232 \\
&= 0.420e^{-0.0456PI} \text{(Residual/Saprolite soil)} \quad r^2 = 0.486
\end{aligned}$$

$\sigma_m^{'}$ = mean effective confining stress

$$= \left(\frac{1 + 2K_o^{'}}{3}\right)\sigma_{v0}^{'}$$

where,

$\sigma_v^{'}$ = vertical effective stress

$\sigma_h^{'}$ = horizontal effective stress

$K_o^{'}$ = coefficient of effective earth stress at rest

$$= \sigma_h^{'}/\sigma_v^{'}$$

It should be noted that the coefficient of determination (R^2) reported in the fitting of the functions of the variable is considerably < 0.9, although the final comparison of measured and calculated G/G_{max} is improved at R^2 = 0.792, 0.841 and 0.930 for Quaternary, Tertiary and residual/saprolite soils, respectively.

2.6 Kishida [8]/[9]

Dynamic behaviour of organic and inorganic cohesive soils was researched in the PhD study by Kishida [10] from a database of 98 cyclic triaxial and resonant column/torsional shear tests on soils from the Sacramento–San Joaquin Delta, USA [8]. The regression model differs from others in that it attempts to predict directly shear modulus (G) from the variables of cyclic shear strain (γ_c), effective vertical confining stress ($\sigma_{vo}^{'}$) and plasticity index (PI). The basis of the model came from a study on dynamic behaviour of highly organic soils [10] and later adapted for cohesive soils [9].

$$\begin{aligned} ln\,G &= b_0 + b_1X_1 + b_2X_2 + b_3X_3 + b_4X_4 \\ &+ b_5(X_1 - \overline{X}_1)\cdot(X_2 - \overline{X}_2) + b_6(X_1 - \overline{X}_1)\cdot(X_3 - \overline{X}_3) \\ &+ b_7(X_2 - \overline{X}_2)\cdot(X_3 - \overline{X}_3) \\ &+ b_8(X_1 - \overline{X}_1)\cdot(X_2 - \overline{X}_2)(X_3 - \overline{X}_3) \end{aligned} \tag{6}$$

where X_1, X_2, X_3 and X_4 are transformed predictor variables of γ_c (in %), σ'_{vo}(in kPa), PI (in %) and OCR.

$$X_1 = \ln\,(\gamma_c + \gamma_r) \quad ; X_2 = \ln \sigma'_{vo}$$
$$X_3 = 2\,/\,[1 + \exp\,(PI/22)] \quad ; X_4 = \ln\,OCR$$
$$\bar{X}_1 = -2.5 \quad ; \bar{X}_2 = 4.0 \quad ; \bar{X}_3 = 0.5$$
$$\gamma_r = \exp[b_9 + b_{10}(X_3 - \bar{X}_3)]$$
$$\gamma_1 = 1.0$$

b_0 *to* b_{10} are regression parameters

$$b_0 = 5.25 \quad ; b_1 = -0.937 \quad ; b_3 = -1.45$$
$$b_6 = 0.00 \quad ; b_9 = -2.51 \quad ; b_{10} = -2.77$$
$$b_2 = 1 - 0.5\bar{X}_3\left[1 + \frac{\ln(\gamma_r) - \bar{X}_1}{\ln\left(\gamma_{l/\gamma_r} + \gamma_{c/\gamma_r}\right)}\right]$$
$$b_4 = 0.8 - 0.8X_3$$
$$b_5 = \frac{0.5\bar{X}_3}{\ln\left(\gamma_{l/\gamma_r} + \gamma_{c/\gamma_r}\right)}$$
$$b_7 = -0.5\left[1 + \frac{\ln(\gamma_r) - \bar{X}_1}{\ln\left(\gamma_{l/\gamma_r} + \gamma_{c/\gamma_r}\right)}\right]$$
$$b_8 = \frac{0.5}{\ln\left(\gamma_{l/\gamma_r} + \gamma_{c/\gamma_r}\right)}$$

2.7 Vardanega and Bolton [20]

Vardanega and Bolton analysed data from 67 tests on 21 clays/silts of various PI ranging from 12 to 150% in undrained conditions [20]. A new methodology was proposed to derive the reference strain and curvature parameter power factor (α) from Darendeli's modified hyperbolic equation Eq. (4). The equation is transformed as follows:

$$\frac{G}{G_{max}} = \frac{1}{1 + \left(\frac{\gamma}{\gamma_r}\right)^{\alpha}}$$
$$\rightarrow \frac{G_{max}}{G} = 1 + \left(\frac{\gamma}{\gamma_r}\right)^{\alpha}$$
$$\rightarrow \frac{G_{max}}{G} - 1 = \left(\frac{\gamma}{\gamma_r}\right)^{\alpha}$$
$$\rightarrow \log\left(\frac{G_{max}}{G} - 1\right) = \alpha\log\left(\frac{\gamma}{\gamma_r}\right)$$

The equation is in a linear form, and a simple linear regression exercise can be undertaken to find the best-fit parameters of α and γ_r for the soils from the database. The influence of strain rate effects is also considered in the regression analysis allowing α (using γ_r at G/G_{max} at 0.5 initially) and γ_r to be derived from static or dynamic soil tests.

For γ_r, it is suggested for best fit to the data set:

$$\gamma_r = J\left(\frac{I_p}{1000}\right) \text{in actual numerical values}$$
$$J = 2.2 \text{ for static adjustment.}$$
$$3.7 \text{ for dynamic adjustment.}$$
$$I_p = \text{Plasticity index expressed numerically, e.g. } 0.4$$

For α, it is suggested for best fit to the dataset:

$$\alpha = 0.736 (\text{with static adjustment})$$
$$= 0.943 (\text{with dynamic adjustment}) \tag{7}$$

The analysis also concurs with Kokusho et al. [12] and Vucetic and Dobry [21] on the limited effect of OCR on the shear modulus degradation curve. However, the influence effects of effective stress on G/G_{max} are not addressed.

Table 1 List of soil types

#	Silt (%)	Clay (%)	Kaolin (%)	Bentonite (%)	PL (%)	LL (%)	PI (%)	MDD (Mg/m^3)	SG
CM1X	79	21	100	–	32	63	31	1.317	2.63
CM2X	69	29	80	20	32	67	35	1.259	2.53
CM3X	59	38	60	40	24	79	55	1.419	2.44
CM4X	42	53	20	80	36	105	69	1.172	2.39
CM5X	29	63	–	100	36	110	74	1.157	2.20

3 Materials, equipment and methodology

3.1 Materials utilized

For the experiments, commercially available inorganic bentonite and kaolinite mineral clay were used. Various proportions were then mixed to produce remoulded and reconstituted synthetic cohesive soils of varying PI. The kaolinite was obtained from the company Kaolin Malaysia Sdn. Bhd. The bentonite was industrial grade sodium bentonite sourced from the company Masda Chemical Sdn. Bhd. The proportions for the various mixes are outlined in Table 1. In addition, laboratory tests were conducted to obtain the plastic limit (PL), liquid limit (LL), max. dry density (MDD) and specific gravity (SG) for each soil sample.

3.2 Equipment used and sample preparation

Proctor compaction tests were performed to determine each soil mix's maximum dry density and optimum moisture content. The soil samples are mixed with distilled water to the required moisture content of 33%, hand spooning into the mould in three layers, and compacted by cylindrical metal hammer tamping to achieve a minimum of 90% max. dry density.

Fig. 3 GDS enterprise-level dynamic triaxial testing system utilized for the cyclic triaxial test

Dynamic strain-controlled testing was conducted using a cyclic triaxial device (as shown in Fig. 3) on 50 mm diameter x 100 mm height cylindrical specimens at various conditions to derive the shear modulus behaviour with increasing strain.

Before testing, the soil specimen is first saturated using a back pressure of 290 kPa, applied from the top to ensure a minimum Skempton's B-coefficient of 0.95. A consolidation phase follows the saturation of the sample. Side drains are utilized to accelerate the consolidation process. The axial strain is measured by internal instrumentation provided in the cyclic device. Shear modulus and damping ratio are calculated from the deviatoric stress vs strain data obtained according to ASTM D3999M.

3.3 Experiment programme

For the cyclic triaxial (CT) tests, each specimen was subjected to strain-controlled cyclic loading with axial strain range from 0.001 to 5%. The accepted analysis results are dependent on the quality of the readings. Deviatoric stress is calculated from the cyclic vertical axial load divided by the adjusted sample area.

$$\gamma = \varepsilon/(1+v) \tag{8}$$

$$\mathrm{E} = (L_{\mathrm{DA}}/S_{\mathrm{DA}}) \cdot (L_{\mathrm{s}}/\mathrm{A}) \tag{9}$$

where from cyclic triaxial test readings,

L_{DA} = double amplitude load (kN).
S_{DA} = double amplitude deformation (mm).
L_s = specimen height after consolidation (mm).
A = adjusted area (Section 11.2.2 ASTM D3999M).
E = Young's modulus

The axial strain (ε) is converted to shear strain (γ), assuming a Poisson ratio of 0.5 (typically for saturated undrained conditions). Thus, the secant shear modulus (G) is similarly related to the secant Young's modulus (E).

$$G = E/2(1+v) \tag{10}$$

Each axial strain setting is subject to five load cycles. The shear modulus is derived from the mean value of deviatoric stress vs axial strain from the four load cycles (double amplitude) after the first single amplitude cycle at each strain level. The loading frequency is 1 Hz. The summary of the experiments is outlined in Table 2.

Table 2 Experiment programme

Specimen no.	Type of test	PI (%)	Measured effective stress, σ′ (kPa)
CM1X-xxx0	CT	31	32
CM1X-xxx1	CT	31	91
CM1X-xxx2	CT	31	195
CM2X-xxx1	CT	35	96
CM3X-xxx1	CT	55	95
CM4X-xxx1	CT	69	95
CM5X-xxx0	CT	74	47
CM5X-xxx1	CT	74	90
CM5X-xxx2	CT	74	198

Table 3 Calculated G_{max} from the empirical equation

Specimen no.	e	Plasticity index, PI (%)	Effective stress, σ′ (kPa)	Calculated G_{max} (MPa)
CM1X-xxx0	0.9	31	32	14.06
CM1X-xxx1	0.9	31	91	23.72
CM1X-xxx2	0.9	31	195	34.72
CM2X-xxx1	1.01	35	96	20.34
CM3X-xxx1	0.9	55	95	31.02
CM4X-xxx1	1.04	69	95	20.45
CM5X-xxx0	0.9	74	47	17.04
CM5X-xxx1	0.9	74	90	23.59
CM5X-xxx2	0.9	74	198	34.98

4 Test results

The derived secant shear modulus (G) is plotted against the log cyclic shear strain amplitude (γ).

4.1 Derivation of G_{max} by empirical equations

To normalize the shear modulus, G_{max} is required. Due to the unavailability of in-field tests and bender element/resonant column equipment, G_{max} is derived from established empirical equations for kaolin and bentonite, respectively.

For kaolin, the Hardin and Drnevich equation [3] based on reconstituted kaolinite and Boston Blue Clay tests is used.

$$G_{max} = 1230\ F(e)(\mathrm{OCR})^{K}\bar{\sigma}_o{}^{0.5}a^{b}\ \left(\text{in lb./in}^2\right) \tag{11}$$

where,

$F(e) = (2.973 - e)^2/(1 + e)$

OCR = taken as 1 for reconstituted soil

$\bar{\sigma}_o$ = mean principal effective stress (lb./in^2)

K = parameter dependent on PI of soil

The parameter K can be obtained from Hardin and Drnevich [3]—Table 1. For bentonite, an equation derived from research by Marcuson and Wahls [17] is utilized.

$$G_{max} = 445\ F(e)\ \sigma'_o{}^{0.5}\ \left(\text{in lb./in}^2\right) \tag{12}$$

where,

$F(e) = (4.4 - e)^2/(1 + e)$

σ'_o = effective stress $\left(\text{lb./in}^2\right)$

The void ratio, e, for the soil sample is obtained from the oedometer test. G_{max} for samples CM2X to CM4X was proportioned from that of kaolin and bentonite. G_{max} values of various PI and effective stress are outlined in Table 3. Figure 4 shows hysteretic loops (stress–strain curves) typically obtained from the cyclic triaxial test.

4.2 PI influence on shear modulus

The effect of varying PI on secant shear modulus, as shown in Fig. 5, clearly follows other established regression models, showing shear modulus increase for the same strain measured as PI increases.

4.3 Effective stress influence on Shear modulus

The following figures (Figs. 6, 7) show shear modulus increase for the same strain measured as effective stress increases for kaolin and bentonite.

5 Derivation of the fitted model

The hyperbolic relationship by Hardin and Drnevich [3], and which was further developed by Darendeli [1], Zhang et al.[23], and Vardanega and Bolton [20] is still retained as

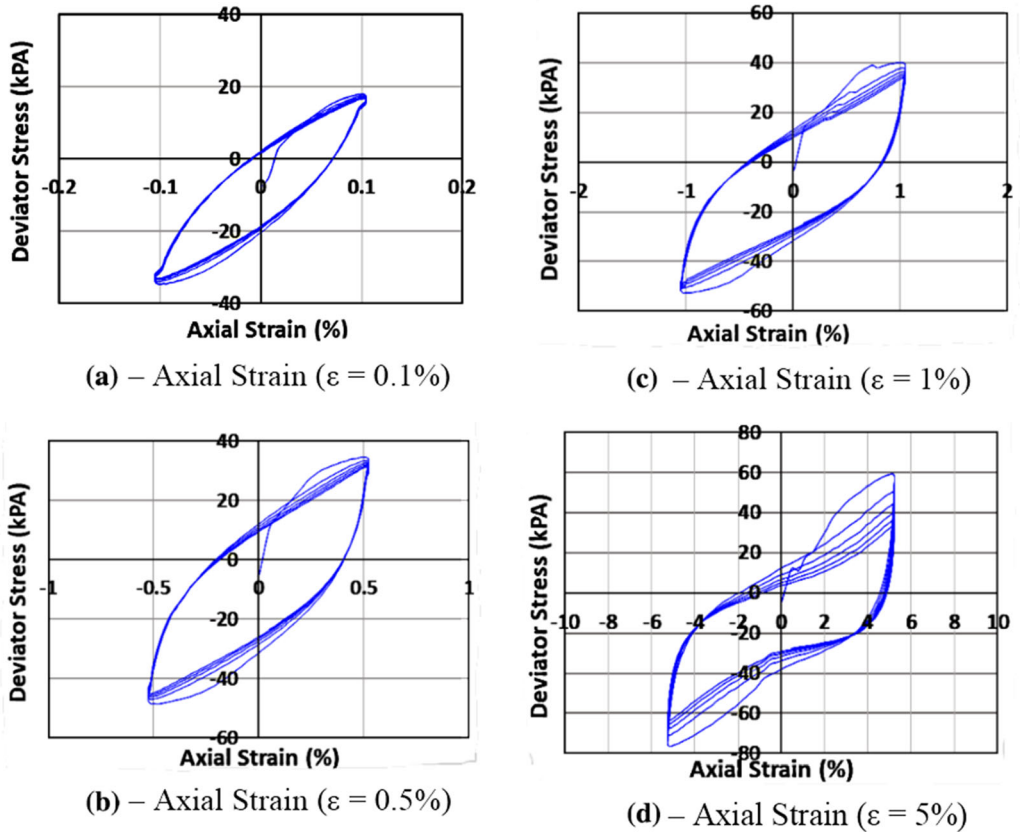

Fig. 4 Results of cyclic test (CM1X-xxx1)

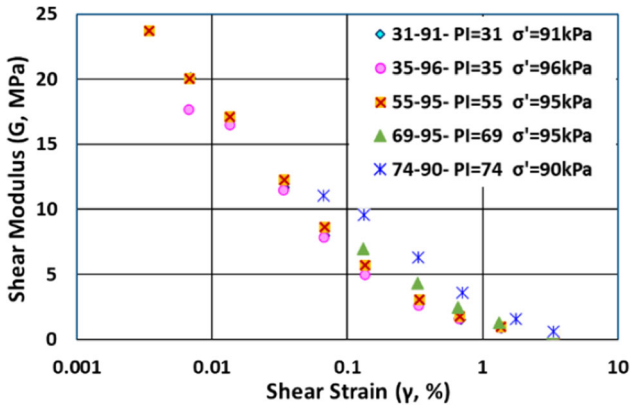

Fig. 5 Effect of plasticity index on shear modulus, G

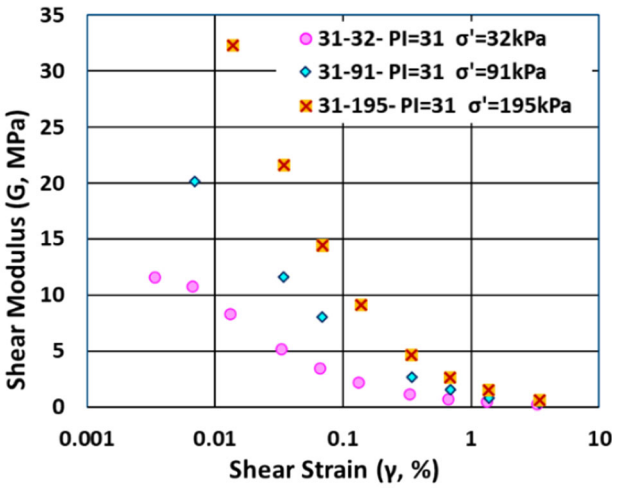

Fig. 6 Influence of effective stress on shear modulus, G for kaolin (PI = 31)

all past research results have validated the basic shape of the shear modulus curve. However, it is proposed to extend the equation in terms of shear strain (γ), plasticity index (PI) and effective stress (σ') with the following:

- Insertion of a fitting function for plasticity index, f (PI).
- Insertion of a fitting function for effective stress, f (σ').
- Removal of the need to derive reference strain.
- Replacement of the original curvature parameter, α, by Darendeli [1] with a new effective stress-influenced parameter curvature function, Z.

The proposed new form of equation shall be as follows:

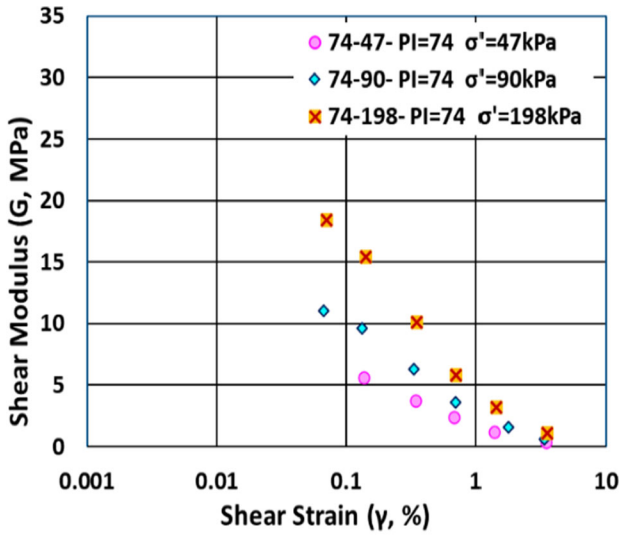

Fig. 7 Influence of effective stress on shear modulus, G for bentonite (PI = 74)

$$\frac{G}{G_{max}} = \frac{1}{1 + f(PI).f(\sigma').(\gamma)^{Z}} \tag{13}$$

The curvature parameter, α, originally fixed at 0.919 [1], is now replaced by a new curvature function, Z, influenced by both PI and effective stress. The effect from OCR variation is not considered due to previous research reporting its insignificant effect on G/G_{max} [12, 21]. Recent studies by Wichtmann and Triantafyllidis [22] have also reported no clear correlation between OCR and effective stress paths when conducting cyclic triaxial tests. Both G and γ are obtained from the conversion of cyclic triaxial test measurements of deviatoric stress and axial strain.

5.1 Fitting function *f* (PI) for the influence of plasticity index

Firstly, the influence of effective stress is fixed by considering samples at fixed σ' of 100 kPa, leaving only the PI's effect to determine f (PI). Since the experiment sample PI range is only limited from PI = 31 to 74, additional values at PI = 0, 15, 85, 100 and 150 are derived from the hyperbolic model by Darendeli [1] to extrapolate additional values for a better definition of the relationship between f (PI) and PI. Darendeli's model values were selected as it was already noted that the increase due to σ' does not decrease as PI increases beyond 100 [9]. Finally, from regression analysis, the f (PI) values, when plotted against PI, fitted to an asymmetrical sigmoidal function as below. Figure 8 shows the fitting function f (PI) vs PI.

$$f(PI) = a1 + (a2 - a1)/\left(1 + (PI/c1)^{b1}\right)^{m1} \tag{14}$$

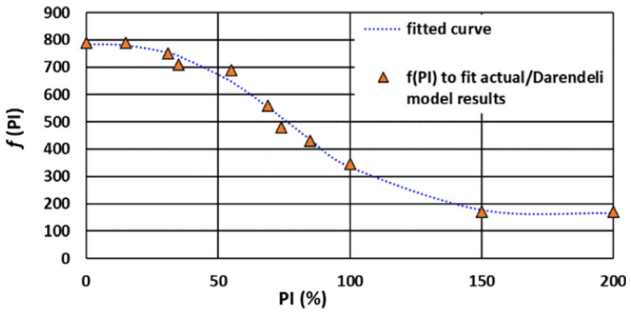

Fig. 8 Parameter, f (PI) vs PI (σ' = 100 kPa)

where,

$a1 = 165.2315$; $a2 = 785.1011$

$b_1 = 2.751255$; $c1 = 60600.94$; $m1 = 58536190$

with a coefficient of determination (R^2) = 0.992.

5.2 Fitting function *D* (σ') for the influence of effective stress

For the influence of effective stress, the soil samples' plasticity index is fixed by considering samples at a fixed PI, leaving only the effect of σ' to determine f (σ'). Again, since the sample σ' range at PI = 31 is only limited to σ' = 50, 100 and 200 kPa, additional values at σ' = 4, 8 and 16 atm using equations from Darendeli's [1] model are included to provide additional values to define better the relationship between f (σ') and σ'.

Lanzo et al. [15] observed that G/G_{max} increases as effective stress increases at soils with low PI, but the effect diminishes as PI increases. The observation is repeated by Likitlersuang et al. [16], who plotted strain increase due to increasing mean effective stress becoming negligible for PI beyond 100. Kishida [9] stated that in the Darendeli regression model, G/G_{max} continues to rise with increasing PI without diminishing at high PI. Therefore, it is necessary to introduce a reducing function to reduce the effect until it becomes insignificant beyond PI = 100. Although f (σ') can be derived using Darendeli model values, it must be further modified to account for the diminishing effect and insignificance beyond PI = 100 (discussed in 5.4). Hence, the function, D (σ'), for the effect of σ' without the diminishing effect from PI above 100% is first derived. Then, regression analysis was performed whereby the values were found to fit an exponential function form as shown in Fig. 9.

$$D(\sigma') = d1 + d2 \cdot e^{(c2 \cdot \sigma')} \tag{15}$$

with the following fitting constants: d1 = − 0.10; d2 = 8.826902; c2 = − 1.134872. σ' is in units of (atm) with a coefficient of determination (R^2) = 0.957.

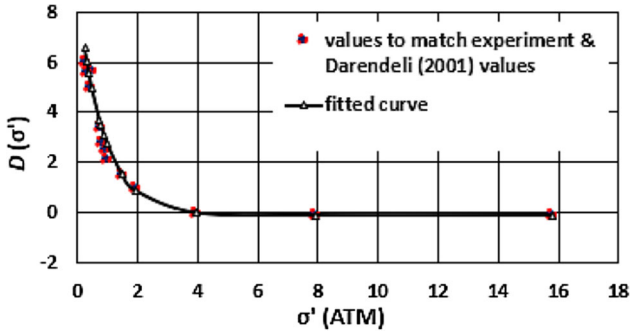

Fig. 9 Parameter, D(σ') vs σ' (PI = 31)

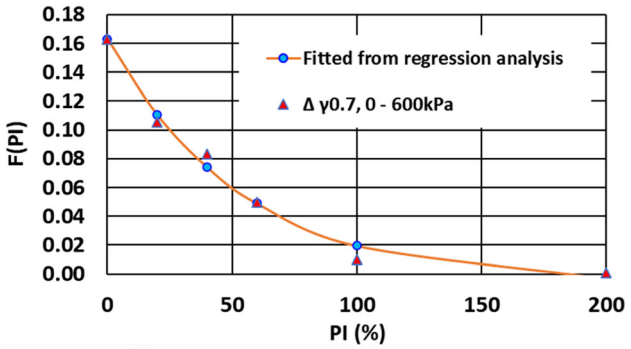

Fig. 10 Parameter, F (PI) vs PI at $\gamma_{0.7}$

5.3 Shaping function *z* (σ') for the influence of effective stress

Both Darendeli [1] and Vardanega and Bolton [20] proposed fixed values for the curvature parameter in their models based on mean values from the range of soils in their studies. However, the experiment results indicate that the curvature of the normalized model is also influenced by effective stress. Therefore, a new curvature function, z (σ'), is proposed to replace α. To investigate the correlation between curvature and effective stress, samples at a fixed PI are considered leaving only the effect of σ' to determine z (σ'). Once again, a combination of experimental results and additional values at σ' = 4, 8 and 16 atm using Darendeli's model equations [1] is included to define better the relationship between z (σ') and σ'.

$$z(\sigma') = d3 + d4 \cdot e^{(c4 \cdot \sigma')} \quad (16)$$

where the following are the fitting constants: d3 = − 0.809; d4 = 0.211; c4 = − 0.008. σ' is in units of kPa with a coefficient of determination (R^2) = 0.927.

5.4 Reducing the influence of effective stress with increasing PI

As mentioned in section 5.2, Lanzo's et al. [15] observation that G/G_{max} increases as effective stress increases at soils with low PI, but the effect diminishes as PI increases was validated by Likitlersuang et al. [16], who plotted strain increase due to increasing mean effective stress becoming negligible for PI beyond 100. Kishida [9] noted that the Darendeli regression model, G/G_{max} continues to rise with increasing PI without diminishing at high PI. Hence, the necessity to introduce a reducing function to reduce the effect until it becomes insignificant beyond PI = 100. Likitlersuang et al. [16] produced a chart for the variations of strain at G/G_{max} = 0.7 ($\gamma_{0.7}$) for a PI range of 0 to 200 and the mean effective stress (σ'_m) ranging from 1 to 600 kPa, together with values by Vucetic and Dobry [21], Ishibashi and Zhang [4], and Teachavorasinskun et al. [19]. The increase in strain with increasing σ'_m up to PI = 100 can be expressed in a asymptotic function, H(PI), which is 1 minus the normalized ratio between the difference of $\gamma_{0.7}$ at σ'_m = 0 kPa and at 600 kPa at a particular PI/difference of γ0.7 at σ'_m = 0 kPa and at 600 kPa at PI = 0. Four different points are plotted for this normalized ratio at PI = 0 (where normalized ratio = 0, 20, 60 and 100). When regression analysis is applied, the values can be fitted to an exponential function for the normalized ratio. The difference in strain, $\Delta\gamma_{0.7}$ at σ'_m = 0 kPa and at 600 kPa fits, follows an exponential function, F(PI), as shown in Fig. 10, where:

$$F(PI) = d_a + d_b \cdot e^{c_a \cdot PI} \quad (17)$$

where the following are the fitting constants:d_a = – 0.007381; d_b = 0.170501; c_a = – 0.018464. PI is in %—e.g. 20%, 30%, etc. with a coefficient of determination (R^2) = 0.989.

The difference in strain is normalized at F(PI)/F(PI = 0), and H(PI) is $1 - F(PI)/F(PI = 0)$.

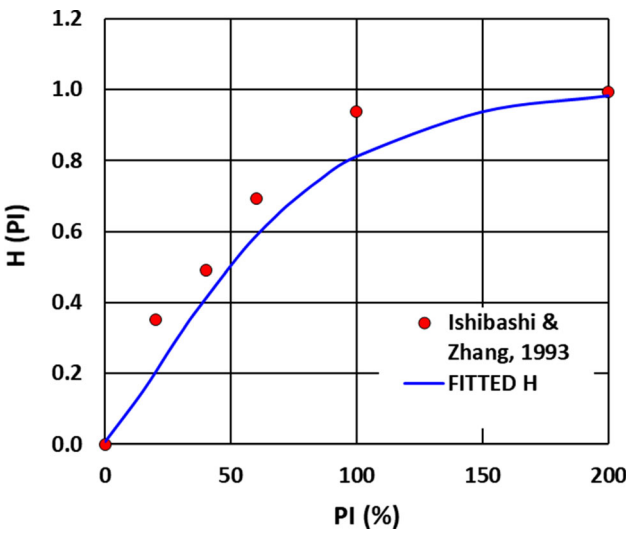

Fig. 11 H(PI) vs PI to reduce the effect of effective stress with PI

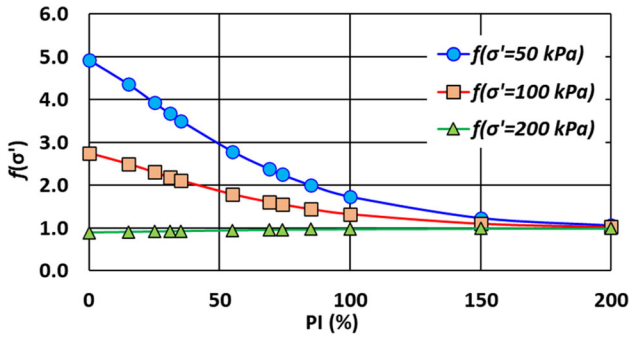

Fig. 12 Parameter $f(\sigma')$ vs PI for various σ′

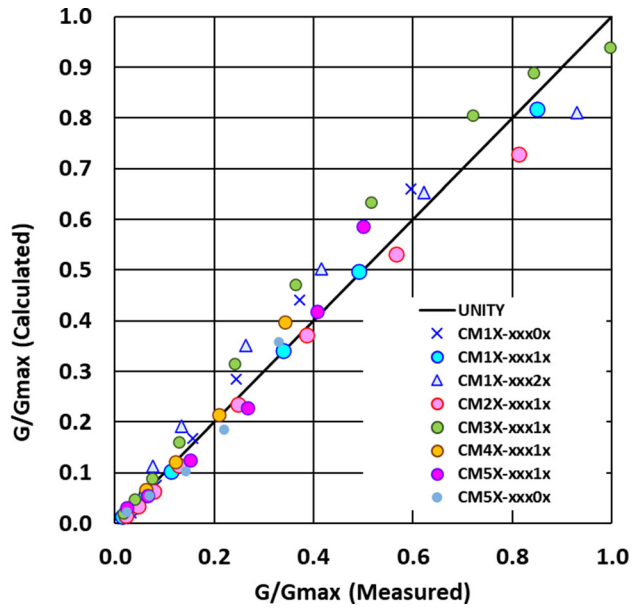

Fig. 13 Comparison of calculated and measured G/G_{max}

H(PI) can be further smoothened to fit a sigmoidal function form through regression analysis as shown in Fig. 11 and represented mathematically as follows:

$$H(PI) = a3 + (a4 - a3)/\left(1 + (PI/c3)^{b2}\right)^{m2} \quad (18)$$

where the following are the fitting constants:

$a_3 = 1.002608;\ a_4 = 0.0081622;\ b2 = 1.25.$

$c_3 = 6378562;\ m2 = 1575318.$

PI is in %—e.g. 20%, etc., with a coefficient of determination (R^2) = 0.90.

The fitting function, $f(\sigma')$, and curvature function, Z, for effective stress can now be expressed as:

$$f(\sigma') = D(\sigma') + H(PI) \cdot (1 - D(\sigma')) \quad (19)$$

$$Z = z(\sigma') + H(PI) \cdot (1 - z(\sigma')) \quad (20)$$

Figure 12 shows the plot of $f(\sigma')$ for various values of PI. The above equations may be applied for any combination of soil plasticity index (PI) and effective stress (σ′) above 50 kPa.

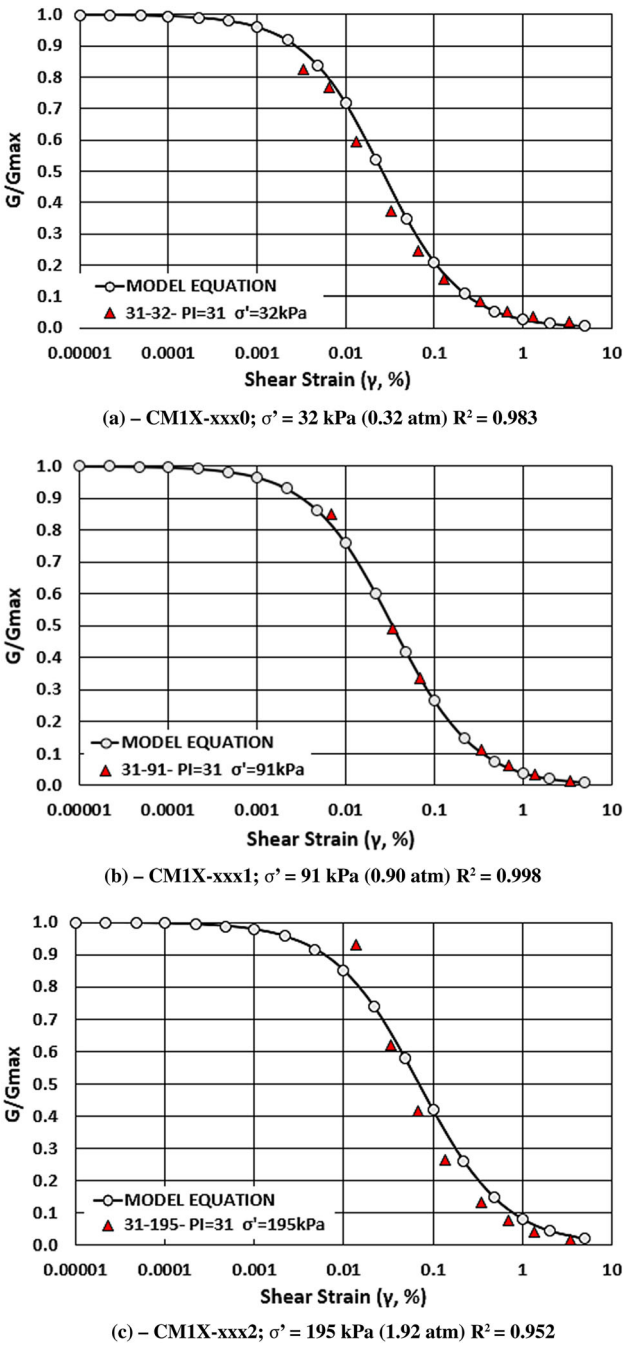

Fig. 14 Comparison of calculated and measured G/G_{max} at PI = 31 for varying effective stress (σ′)

5.5 Comparison with experimental results

The proposed model equation compares well with the experimental results performed. Figure 13 shows the

calculated G/G_{max} vs experimental result G/G_{max} values with the calculated coefficient of determination (R^2) values of 0.968 overall. Most of the residuals between calculated and measured values come from samples CM2X-xxx1x (80% K/20% B) and CM3X-xxx1x (60% K/40% B). Noticeable scatter from both mentioned samples occurs from $G/G_{max} > 0.5$ onwards. The scatter may be attributed to (1) consistency limitations of cyclic triaxial device measurement at smaller strains $< 0.1\%$ and (2) a low number of experiment values. Consistent readings for cyclic triaxial tests are generally limited to strains $> 0.1\%$. In order to obtain better readings below 0.1% strain, resonant column (RC) tests would need to be conducted.

In Fig. 14, calculated G/G_{max} values are compared against experimental results at varying effective stress (σ' = 50, 100 and 200 kPa). A close fit is achieved with high R^2, even for a low number of experimental values.

Likewise, in Fig. 15, the calculated G/G_{max} values are compared against experimental results at varying PI.

5.6 Comparison with other regression models

The proposed model equation is compared with the other regression models discussed. When comparing at fixed effective stress of 100 kPa, the following can be observed:

- For lower values of the plasticity index, ranging from PI = 0 to 35, regression models are closely aligned together. The model equation is also compared to the average G/G_{max} (global strain) results for Brahmaputra sand (PI = 0) [14] from studies by Kumar et al. [13] and found to be in good agreement.
- As PI increases, models start to diverge noticeably from each other to form into two distinct groups.
- Group 1—comprising Ishibashi and Zhang [4] and Zhang et al. [23].
- Group 2—comprising Vucetic and Dobry [21], Kishida [8, 9], and Vardanega and Bolton [20].

The Darendeli model [1] is positioned approximately midway between the two groups. Finally, the basic

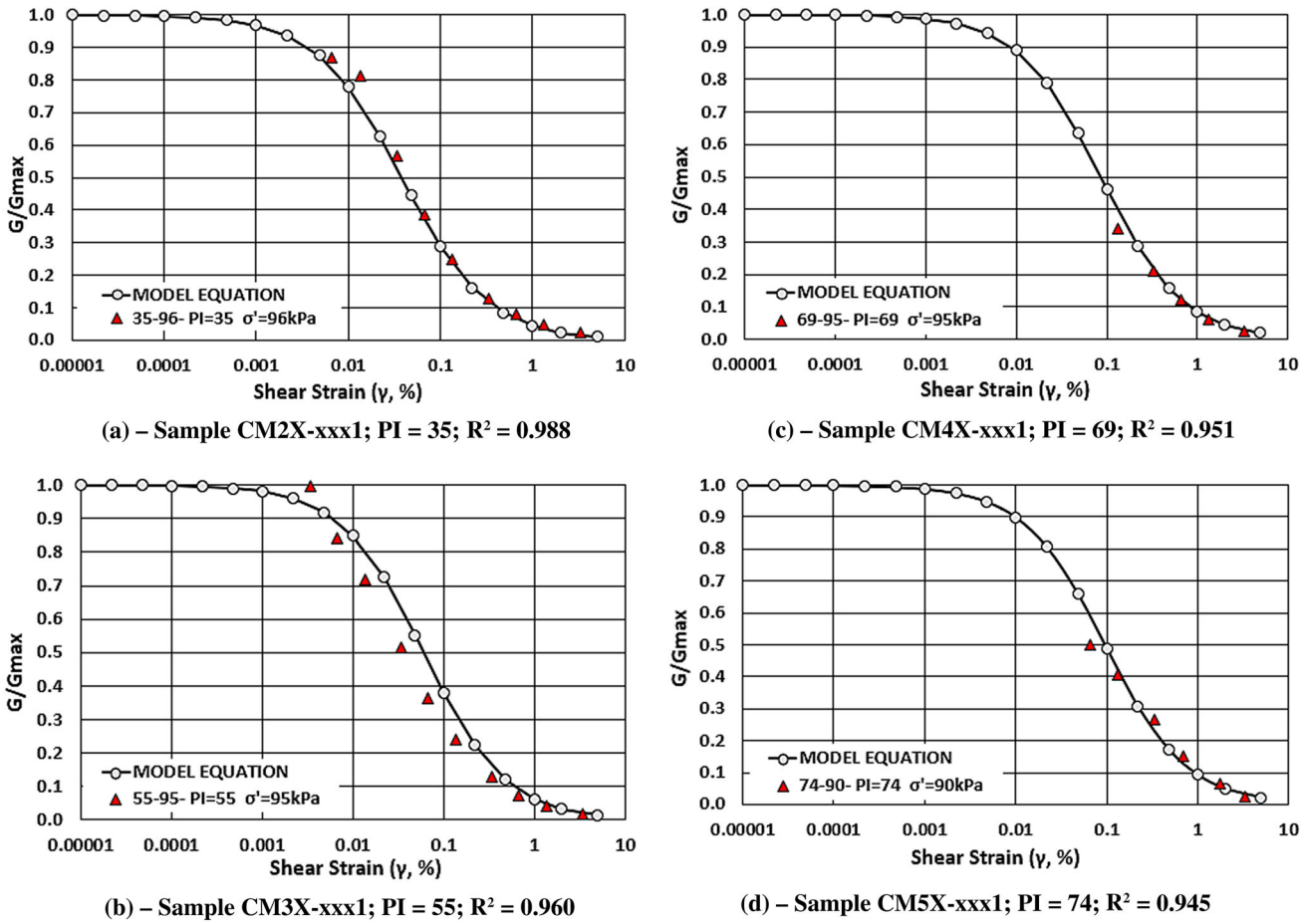

(a) – Sample CM2X-xxx1; PI = 35; R^2 = 0.988

(c) – Sample CM4X-xxx1; PI = 69; R^2 = 0.951

(b) – Sample CM3X-xxx1; PI = 55; R^2 = 0.960

(d) – Sample CM5X-xxx1; PI = 74; R^2 = 0.945

Fig. 15 Comparison of calculated and measured G/G_{max} for various PI

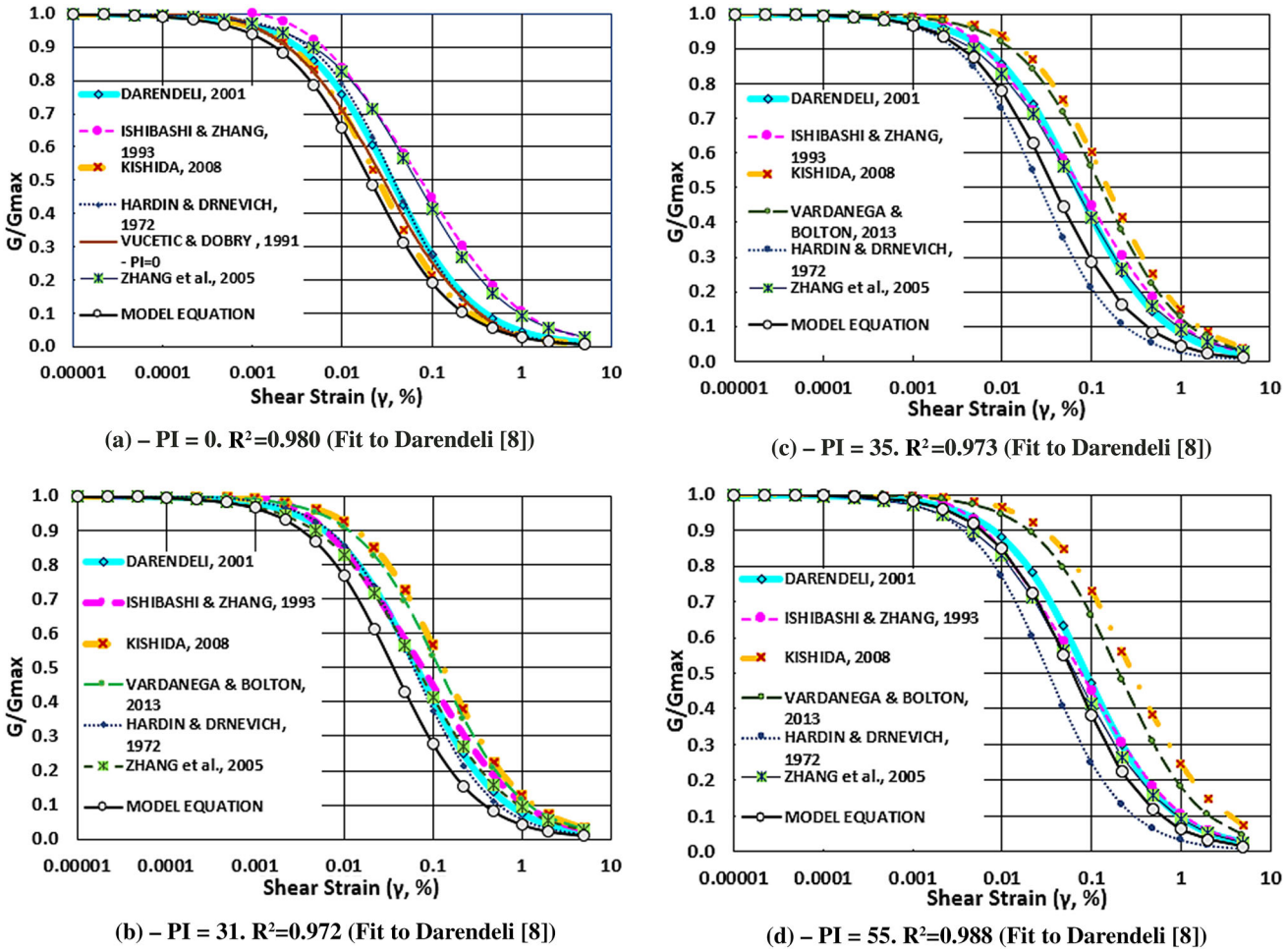

(a) – PI = 0. R^2=0.980 (Fit to Darendeli [8])

(c) – PI = 35. R^2=0.973 (Fit to Darendeli [8])

(b) – PI = 31. R^2=0.972 (Fit to Darendeli [8])

(d) – PI = 55. R^2=0.988 (Fit to Darendeli [8])

Fig. 16 Comparison of regression models based on σ' = 100 kPa (PI 0 to 55)

hyperbolic model by Hardin and Drnevich [3] is essentially dependent on the reference strain, which is tied to experimental results and only appears in the charts for PI = 31, 35, 55, 69 and 74.

Figure 16 shows a consistently good fit of the proposed model equation to the other regression models gradually approaching convergence with the Darendeli model curve.

The proposed model curve degradation slope is generally aligned for all models except for Hardin and Drnevich, which utilized a curvature parameter of 1 and Vardanega and Bolton [20].

Referring to Fig. 16a and b, for PI = 31 and 35, the proposed model equation is at the lower bound of Group 1 models because the mathematical fitting was tied closely to the test results obtained.

After that, the proposed model equation agrees closely with Group 1 and Darendeli [1] from PI = 35 to 74 and starts to move towards aligning with Group 2 from PI = 100 onwards, where Kishida [8, 9], Vardanega and Bolton [20], and Vucetic and Dobry [21] models have the least biases and are considered more accurate [9].

In Fig. 17, the model equation continues to match the Darendeli model [1] and, as designed to, moves to align closer with the Kishida model [9] when soil PI exceeds 100. As shown in Figs. 16 and 17, the close fit demonstrates the model equation's ability to accommodate a wide range of plasticity index values from PI = 0 to 200 within the lower and upper bounds of the regression models.

5.7 Design curves for various effective pressures

To demonstrate the effectiveness of the reducing function, H(PI), in limiting the influence of increasing effective pressure as PI increases, design curves are plotted for various PI with effective stresses of σ' = 50–100–200 kPa (0.49–0.99–1.97 atm) in Fig. 18. The curves clearly show H (PI)'s limiting effect as the influence (measured by the gap between σ' = 50 and σ' = 200) diminishes to negligible values beyond PI = 100.

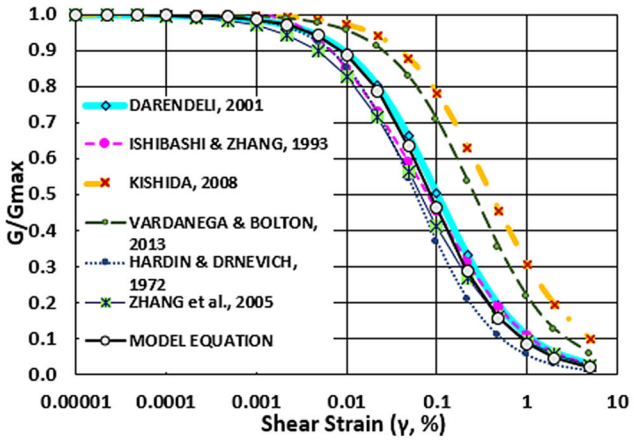

(a) – PI = 69. R^2=0.997 (Fit to Darendeli [8])

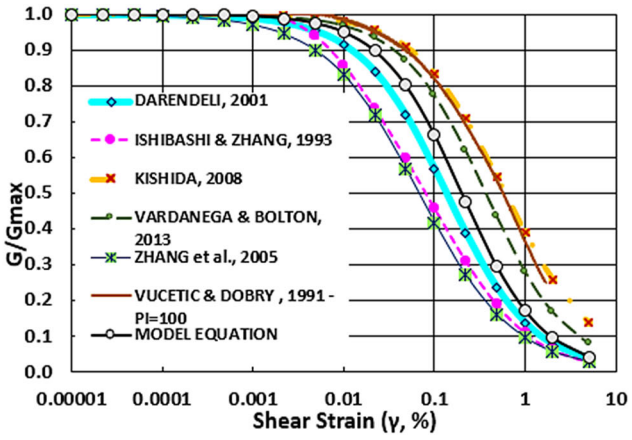

(c) – PI = 100. R^2=0.985 (Fit to Darendeli [8])

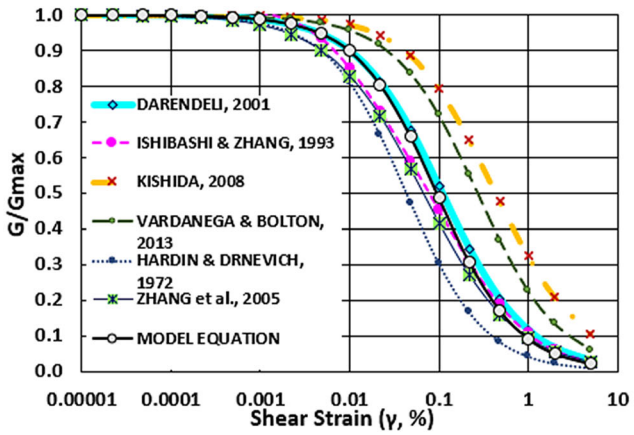

(b) – PI = 74. R^2=0.998 (Fit to Darendeli [8])

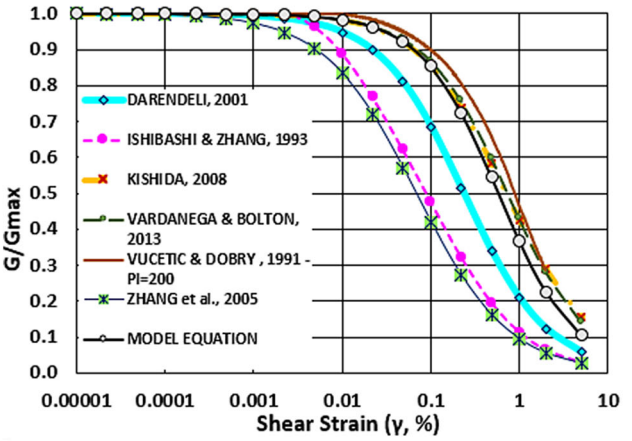

(d) – PI = 200. R^2=0.991 (Fit to Kishida [12])

Fig. 17 Comparison of regression models based on σ' = 100 kPa (PI 69 to 200)

6 Discussion

The proposed model seeks to incorporate both aspects of the Darendeli model, developed from Hardin and Drnevich, which appears more suited with lower bias at lower PI and the Kishida model, which exhibited advantages over the other models for higher soil PI values [9].

Firstly, the divergence into two distinct groups may be explained through the basis from which the results' database is obtained to derive the regression models.

Group 1 comprises models that are based initially on experiments of non-cohesive soils—e.g. Ishibashi and Zhang [4], who adapted their model from non-plastic soils and Zhang et al. [23], which based the model on the research of soils grouped by geologic age—Quaternary/Tertiary and non-age-specific residual/saprolite soils.

Group 2 consists of models developed from results derived from a higher plasticity cohesive soils research database—e.g. Vucetic and Dobry [21] and Vardanega and Bolton [20]. In Kishida [8], the regression model was originally adapted from equations developed for organic soils with high plasticity.

Thus, it can be postulated that Group 1 models are more suited towards non-cohesive and lower PI soils, whereas Group 2 is optimized towards high PI soils. Kishida [9] also reports on biases with PI for the different models. The model developed by Darendeli [1] is positioned between the two groups. Darendeli [1] tested various soils ranging from non-plastic PI = 0 to 53 with only two other soil samples higher at 79 and 132. It also underestimates G/G_{max} for higher PI but not to the same extent as Group 1 models. Kishida's model [8] refers to Vucetic and Dobry's [21] model to accuracy. However, Vucetic and Dobry's model does not include the effect of effective stress on G/G_{max} [1, 9]. Moreover, G_{max} derived using the Kishida model equations differs considerably from the established empirical equations [3, 17] for kaolin and bentonite soil.

The established empirical equations are validated because they were utilized to create the normalized curves from experimental shear modulus results for PI = 31, 35,

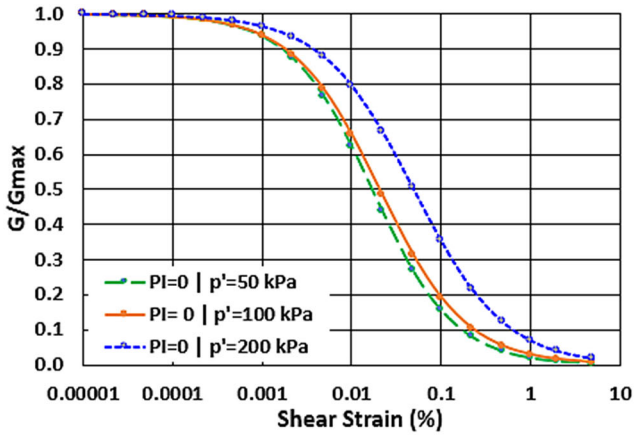

(a) – Effect of varying effective stress at PI = 0

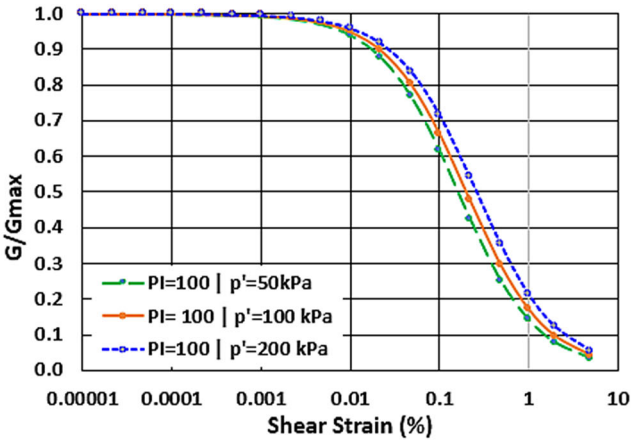

(c) – Effect of varying effective stress at PI = 100

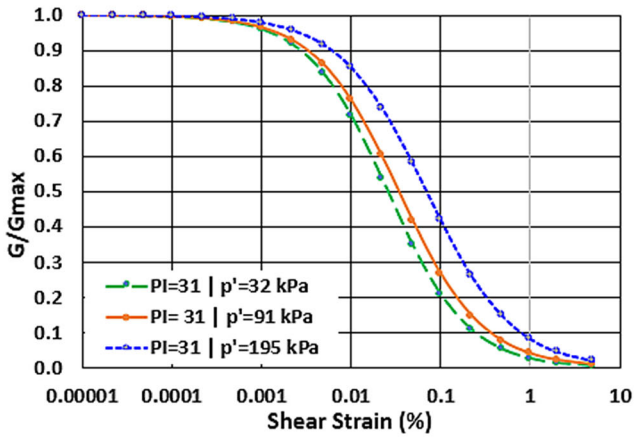

(b) – Effect of varying effective stress at PI = 31

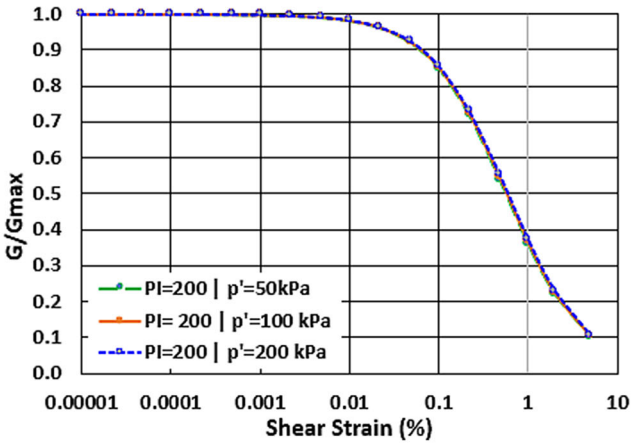

(d) – Effect of varying effective stress at PI = 200

Fig. 18 Comparison of model equation based on σ' = 50–100-200 kPa (0.49–0.99–1.97 atm)

55, 69 and 74. These proposed model curve results match very well, showing high coefficients of determination (R^2) to Darendeli's model for soil PI up to 100 and Kishida's model for soil PI above 100.

Secondly, the Darendeli [1] and Zhang et al. [23] models continue to increase when applied with high PI values showing increasing effective stress beyond the threshold of 100 in conflict with the observations by Likitlersuang et al. [16]. This conflict is rectified in the proposed extended model equation by introducing the limiting function, H(PI). H(PI) effectively reduces any further increase in G/G_{max} to insignificant magnitudes beyond PI = 100, in alignment with the findings of Likitlersuang et al. [16]. The reducing effect from H(PI) is clearly shown in Fig. 18, with the influence of effective pressure variation becoming insignificant beyond PI = 100. Kishida proposed that the reducing effect of σ' with increasing PI could be related to soil compressibility [9].

Thirdly, the observation of differing values for the curvature parameter, α, can now be resolved by replacing α with a new curvature function that considers the influence of effective stress and soil plasticity index. Darendeli [1] set the value of α at 0.919 as the mean value from various soils tested. However, actual α varied between soil groups (from clean sands to silts to clays) tested. Vardanega and Bolton [20] proposed an updated α value of 0.943 with a $\pm$ 30% margin for 90% of the soil data studied. The differing values for α suggest a possible relationship between soil PI and α.

Experiment results also showed a correlation between the curvature parameter and effective stress for a given PI. Hence, a curvature function Z is proposed to replace the curvature parameter, α. Initially, a curvature function at a fixed PI, $z(\sigma')$, is established. After that, the limiting effects beyond the value of PI = 100 are imposed by similarly introducing the limiting function, H(PI), to develop the corrected curvature function, Z (Eq. 20).

Finally, the proposed model equation (Eq. 13) dispenses with the need for a reference strain. Instead, the mathematically fitted extended model only requires the plasticity

Table 4 Qualitative comparison of models

Model	Mathematical function	Influence factors		
		Reference strain (γ_r)	Plasticity index (PI)	Effective stress (σ')
Hardin and Drnevich [3]	Basic hyperbolic	Requires γ_r	No, based only on strain increase	No, based only on strain increase
Vucetic and Dobry [21]	No mathematical function	N/A	Yes	No effect with a change in σ' as PI increases
Ishibashi and Zhang [4]	Non-Hardin hyperbolic	No γ_r	Very small effect with a change in PI	No effect with a change in σ' as PI increases
Darendeli [1]	Modified Hardin hyperbolic	Requires γ_r	Increases as the PI increases Fixed shaping parameter	Yes—increases with an increase in σ'. Continues increasing beyond PI = 100
Zhang et al. [23]	Modified Hardin hyperbolic	Requires γ_r	No effect with a change in PI	Yes—small effect with a change in σ'. Continues increasing beyond PI = 100
Kishida [8]	Direct derivation of shear modulus, G	Requires γ_r	Increases as the PI increases	Very small effect with a change in σ' up to PI = 100, after that, negligible effect
Vardanega and Bolton [20]	Modified Hardin hyperbolic	Requires γ_r	Increases as the PI increases Fixed shaping parameter	No effect with a change in σ' as PI increases
Extended Model equation proposed (Eq. 13)	Extended Darendeli hyperbolic	γ_r not required	Increases as the PI increases The shaping function considers the effect of PI	Increases as σ' increases up to PI = 100, after that negligible effect The shaping function considers the effect of σ'

index (property of the soil) and effective stress (depth of the soil) to define the relationship between shear modulus and shear strain. The plasticity index of soil can be readily determined from laboratory tests for Atterberg limits, whereas the effective stress can be derived after considering the elevation of the groundwater level and density of the different soil layers. Table 4 summarizes the comparison of the different regression models.

7 Conclusion

Soil G/G_{max} vs shear strain behaviour models have been extensively researched with several different approaches. The primary influence factors for the behaviour are shear strain (γ), effective stress (σ') and plasticity index (PI).

Other influence factors are not substantive enough to affect the behaviour significantly. However, model prediction differences can become substantial when influence factors diverge from experiment values on which the research is based. Furthermore, previous reviews have identified omissions or non-considerations of the effect of influence factors in the different regression models developed to date.

The established regression models discussed can be divided into Group 1 using the non-cohesive soils model and Group 2, based on higher PI cohesive soil. Both groups agree closely at low PI but begin to differ as PI increases, significantly when beyond 100. The authors propose extending the Darendeli model further with fitting functions to represent better the spectrum of PI (from 0% onwards) and effective stress (from 50 kPa onwards) for cohesive soils.

The proposed model also has the advantage of referencing the primary influence factors developed mathematically, considering previous models' combined research findings. The diminishing influence of effective stress at soil PI beyond 100% has been incorporated into this extended model, and the need for the reference strain is removed. Experiments conducted have also revalidated the empirical equations for G_{max} by its close fit of the derived G/G_{max} vs strain curves. The calculated values of G/G_{max} from the proposed model are in close agreement with experimental values. In addition, the proposed extended model compares favourably with the Kishida regression model, which is considered to have lower biases at higher soil PI. It is hoped that the proposed model can be utilized to facilitate the preliminary prediction of shear modulus with increasing strain. Future research identified to refine the model further is as follows:

- The curvature power parameter (α), which was the average for all soils studied by Darendeli [1], has now been replaced by a curvature function (Z). However,

additional tests are recommended to refine and validate this function due to the low number of experiments.
- Due to the limited number of experiments performed, the soil research database should be expanded to validate the model further.
- The reducing effect of effective stress on G/G_{max} could be further investigated by correlating it with soil compressibility (e.g. coefficient of soil compressibility) obtained from soil oedometer tests.
- A relationship between soil compressive strength (q) and elastic modulus (E) with shear modulus may be studied.
- A corresponding model for the damping ratio of soils vs strain can similarly be developed from the methodology used in this article.
- Studies to apply the model for improved or stabilized soil (e.g. soil stabilization) can be conducted. By increasing binder dosage, compressive strengths can approach conventional mass or weak concrete. Thus, the constitutive model may transition from regular soil to hard soil soft rock (HSSR). Research is needed to establish a crossover point.

Acknowledgements The authors would like to acknowledge the following for their support and assistance: The University of Nottingham Malaysia, Faculty of Science and Engineering, Department of Civil Engineering. Soilpro Technical Services Sdn Bhd (Malaysia), from which experiments were conducted. www.mycurvefit.com for curve-fitting resources.

Funding No funding was provided for this research article.

Declarations

Conflict of interest The authors declare that the article was conducted in the absence of any commercial or financial relationships that could be construed as a potential conflict of interest.

References

1. Darendeli MB (2001) *Development of a new family of normalized modulus reduction and material damping curves*. PhD thesis. University of Texas, Austin, TX, USA, 2001
2. Diaz-Rodriguez JA, Lopez-Molina JA (2008) Strain Thresholds in Soil Dynamics. Presented at the 14WCEE, Beijing, China
3. Hardin BO, Drnevich VP (1972) Shear modulus and damping in soils: design equations and curves. J Soil Mech Found Div 98(sm7):667–692
4. Ishibashi I, Zhang X (1993) Unified dynamic shear moduli and damping ratios of sand and clay. Soils Found 33(1):182–191. https://doi.org/10.3208/sandf1972.33.182
5. Iwasaki T, Tatsuoka F, Takagi Y (1978) Shear moduli of sands under cyclic torsional shear loading. Soils Found 18(1):39–56. https://doi.org/10.3208/sandf1972.18.39
6. Kallioglu P, Tika Th, Pitilakis K (2008) Shear modulus and damping ratio of cohesive soils. J Earthq Eng 12(6):879–913. https://doi.org/10.1080/13632460801888525
7. Karray M, Hussein MN (2017) Shear wave velocity as function of cone penetration resistance and grain size for holocene-age uncemented soils: a new perspective. Acta Geotech 12(5):1129–1158. https://doi.org/10.1007/s11440-016-0520-2
8. Kishida T (2008) *Seismic Site Effects for the Sacramento-San Joaquin Delta*. Univ. of California, Davis, CA
9. Kishida T (2017) Comparison and correction of modulus reduction models for clays and silts. J Geotech Geoenviron Eng 143(4):04016110. https://doi.org/10.1061/(ASCE)GT.1943-5606.0001627
10. Kishida T, Boulanger RW, Abrahamson NA, Wehling TM, Driller MW (2009) Regression models for dynamic properties of highly organic soils. J Geotech Geoenviron Eng 135(4):533–543. https://doi.org/10.1061/(ASCE)1090-0241(2009)135:4(533)
11. Kokusho T (1980) Cyclic triaxial test of dynamic soil properties for wide strain range. Soils Found 20(2):45–60. https://doi.org/10.3208/sandf1972.20.2_45
12. Kokusho T, Yoshida Y, Esashi Y (1982) Dynamic properties of soft clay for wide strain range. Soils Found 22(4):1–18. https://doi.org/10.3208/sandf1972.22.4_1
13. Kumar SS, Krishna AM (2021) Evaluation of monotonic and dynamic shear modulus of sand using on-sample transducers in cyclic triaxial apparatus. Acta Geotech 16(1):221–236. https://doi.org/10.1007/s11440-020-01035-2
14. Kumar SS, Krishna AM, Dey A (2017) Evaluation of dynamic properties of sandy soil at high cyclic strains. Soil Dyn Earthq Eng 99:157–167. https://doi.org/10.1016/j.soildyn.2017.05.016
15. Lanzo G, Vucetic M, Doroudian M (1997) Reduction of shear modulus at small strains in simple shear. J Geotech Geoenviron Eng 123(11):1035–1042. https://doi.org/10.1061/(ASCE)1090-0241(1997)123:11(1035)
16. Likitlersuang S, Teachavorasinskun S, Surarak C, Oh E, Balasubramaniam A (2013) Small strain stiffness and stiffness degradation curve of Bangkok clays. Soils Found 53(4):498–509. https://doi.org/10.1016/j.sandf.2013.06.003
17. Marcuson WF III, Wahls HE (1972) Time effects on dynamic shear modulus of clays. J Soil Mech Found Div 98(SM12):1359–1373
18. Tatsuoka F, Iwasaki T, Takagi Y (1978) Hysteretic damping of sands under cyclic loading and its relation to shear modulus. Soils Found 18(2):25–40. https://doi.org/10.3208/sandf1972.18.2_25
19. Teachavorasinskun S, Thongchim P, Lukkunaprasit P (2002) Shear modulus and damping of soft bangkok clays. Can Geotech J 39(5):1201–1208. https://doi.org/10.1139/t02-048
20. Vardanega PJ, Bolton MD (2013) Stiffness of clays and silts: normalizing shear modulus and shear strain. J Geotech Geoenviron Eng 139(9):1575–1589. https://doi.org/10.1061/(ASCE)GT.1943-5606.0000887
21. Vucetic M, Dobry R (1991) Effect of soil plasticity on cyclic response. J Geotech Eng 117(1):89–107. https://doi.org/10.1061/(ASCE)0733-9410(1991)117:1(89)
22. Wichtmann T, Triantafyllidis T (2018) Monotonic and cyclic tests on kaolin: a database for the development, calibration and verification of constitutive models for cohesive soils with focus to cyclic loading. Acta Geotech 13(5):1103–1128. https://doi.org/10.1007/s11440-017-0588-3
23. Zhang J, Andrus RD, Juang CH (2005) Normalized shear modulus and material damping ratio relationships. J Geotech Geoenviron Eng 131(4):453–464. https://doi.org/10.1061/(ASCE)1090-0241(2005)131:4(453)